Article:

Mantle anisotropy beneath the Earth's mid-ocean ridges

Andy Nowacki*, J-Michael Kendall, James Wookey

School of Earth Sciences, University of Bristol, Wills Memorial Building, Queen's Road, Bristol, BS8 1RJ, UK

Abstract

Observations of seismic anisotropy at oceanic spreading centres offer insights into mid-ocean ridge processes and the formation of new plates. Here, remote observations of seismic anisotropy beneath mid-ocean ridges are made using measurements of source-side shear wave splitting. Over 100 high-quality measurements are made using earthquakes that occur near mid-ocean ridges and transform faults, but are observed at teleseismic distances. In general, for off-axis ridge events, the polarisation of fast shear waves, ϕ'', is approximately parallel to the spreading direction. Nearer the ridge ($\lesssim 50$ km), ϕ'' becomes more scattered and is often ridge-parallel. Delay times, δt, tend to increase from <1 s near the ridge axis to ~3 s further away. Slow-spreading regions (Gakkel and Southwest Indian Ridges) show smaller amounts of splitting than faster spreading centres. At transform zones, the pattern is more complex. Coverage beneath the East Pacific Rise is especially good, and we observe a systematic increase in delay times in S wave splitting measurements compared to previous SKS splitting observations made at ocean-bottom seismometers. One compatible explanation is the presence of horizontally-aligned, connected layers of melt at depth; this is also compatible with other observations of the 'LAB' discontinuity and surface-wave derived measurements of radial anisotropy.

Key words: mid-ocean ridges, seismic anisotropy, LAB, mantle dynamics, LPO

*Corresponding author.
Email address: andy.nowacki@bristol.ac.uk (Andy Nowacki)

1. Introduction

Although it is well known that mid-ocean ridges (MORs) mark sites where oceanic lithosphere is created, there is still considerable uncertainty about mantle processes near ridges and how melt is extracted to form new crust. It has been long understood that viscous shearing leads to the lattice-preferred orientation (LPO) of mantle minerals at spreading centres (e.g., Hess, 1964; Blackman et al., 1996; Tommasi et al., 1999). Additionally, upwelling and decompression lead to melt generation, and shearing and strain partitioning can cause melt segregation (Phipps Morgan, 1987; Holtzman and Kendall, 2010). Both effects can impart a significant anisotropic signature on seismic waves, measurements of which can be therefore used to probe the dynamics of the Earth's upper mantle (UM) beneath ridges.

Measurements of two orthogonally polarised and independent shear waves (i.e., shear wave splitting) are the most unambiguous observation of anisotropy, and are now routinely made in continental regions, or on oceanic islands (for reviews, see for instance Savage, 1999; Long and Silver, 2009). With UM anisotropy, the orientations of fast shear waves, as derived from splitting measurements, are usually interpreted in terms of LPO in peridotites, where olivine a-axes align roughly parallel to mantle flow directions (e.g., Mainprice, 2007). The delay time between the fast and slow shear-waves is proportional to the magnitude of the anisotropy and the extent of the anisotropic region.

Whilst subduction zones and orogens are well sampled, MORs have not been routinely investigated because of significant logistical problems with placing seismometers on the seafloor. Experiments using ocean-bottom seismometers (OBSs) (Blackman et al., 1993, 1995b; Wolfe and Solomon, 1998; Hung and Forsyth, 1999; Barclay and Toomey, 2003; Harmon et al., 2004) have provided vital insights into MOR processes, though there are still very few observations of shear wave splitting at MORs. Using teleseismic phases (e.g., SKS), these few studies generally reveal fast shear wave polarisations parallel to the direction of plate spreading, with increasing values in delay times moving away from the ridge axis (Wolfe and Solomon, 1998; Hung and Forsyth, 1999; Harmon et al., 2004). These observations are consistent with interpretations of olivine LPO as originally proposed by Hess (1964) (based on

observations of P-wave anisotropy) and as modelled by Blackman et al. (1996). In contrast, shallow earthquakes measured within the axial valley show a fast shear-wave orientations in the crust that are parallel to the ridge axis, which are attributed to aligned cracks and layered intrusions of volcanic material (Barclay and Toomey, 2003). Blackman et al. (1996, 1995a, 1993) explained the early arrival of P-waves across the southern Mid-Atlantic Ridge in terms of the vertical alignment on olivine a-axes in a mantle wedge beneath the ridge axis. Subsequent modelling has suggested that the vertical alignment of melt in films, pockets or bands would also be very effective in generating shear-wave splitting in near-vertically arriving teleseismic phases (e.g., Kendall, 1994; Blackman and Kendall, 1997; Holtzman and Kendall, 2010), and would also predict ridge-parallel fast shear-wave polarisations.

Previous studies of anisotropy beneath MORs in a global context have been undertaken using surface waves to infer azimuthal anisotropy (see e.g., Becker et al., 2007). Debayle et al. (2005), for instance, show that beneath MORs, fast orientations are generally similar to the spreading direction, however the behaviour beneath transform zones is more complex and such surface wave studies are limited in their horizontal resolution. It is also the case that even for the simpler case of global inversions for radial anisotropy in the UM, *a priori* corrections for the crust have a strong effect on the results of such inversions (Ferreira et al., 2010). Hence whilst this should be less of a problem in the region of MORs, where the crust is simple, caution in directly interpreting such results is still advisable. In a more localised study Gaherty (2001) and Delorey et al. (2007) mapped vertical and lateral variations in anisotropy beneath the Reykjanes Ridge. Using sources on the Gibbs fracture zone and receivers on Iceland, differences in Love and Rayleigh wave arrival times revealed faster vertically-polarised Rayleigh waves than horizontally-polarised Loves waves near the ridge axis and at depths less than 100 km. This observation is consistent with either the vertical alignment of olivine a-axes or a melt-induced anisotropy, but Holtzman and Kendall (2010) argue that the latter is more likely.

In this study we evaluate MOR anisotropy using measurements of shear wave splitting which occur beneath the earthquake, rather than the receiver, using direct S waves—a technique often termed 'source-side splitting' (e.g., Schoenecker et al., 1997; Nowacki et al.,

58 2010; Foley and Long, 2011). Using seismic stations with well-characterised anisotropy in

59 the UM beneath the receivers, we can remove the effect of the splitting on the receiver side

60 and measure only that which occurs beneath the source. We then attempt to interpret these

61 observations in the context of previous observations and proposed mechanisms for anisotropy

62 beneath a MOR.

2. Methods and data

63

64 *2.1. Shear wave splitting*

65　　We aim to measure the seismic anisotropy beneath MORs around the world using the

66 primary observable it produces, shear wave splitting. We use the 'minimum eigenvalue'

67 technique of Teanby et al. (2004) (which is an extension of that of Silver and Chan (1991)),

68 which removes splitting by effectively maximising the linearity of the horizontal particle

69 motion for a given pair of splitting parameters: the fast direction, ϕ, and the delay between

70 the fast and slow waves, δt. Where measurements are available for an event at more than one

71 station within an azimuthal range of 15°, we use the method of Wolfe and Silver (1998) to

72 stack the small eigenvalue (λ_2) surfaces, with a backazimuth-independent implementation.

73 This significantly reduces the errors when for some stations the measurement is very near

74 null, as the initial polarisation is close to the fast direction beneath the event.

75　　In this study, we make the common assumption that the lower mantle above D″ is not

76 significantly anisotropic: despite some evidence of its presence in the uppermost lower mantle

77 (Wookey and Kendall, 2004), several studies support this assumption (e.g., Meade et al.,

78 1995; Montagner and Kennett, 1996; Panning and Romanowicz, 2006; Kustowski et al.,

79 2008). Hence we can infer that any splitting is caused by anisotropy in the UM beneath the

80 source and receiver. If we have prior knowledge of splitting in the UM beneath the receiver,

81 we may correct for this and analyse the S phase, retrieving the splitting caused by anisotropy

82 beneath the source. We interpret the fast direction of the receiver-corrected signal simply

83 by considering the fast orientation at the source, $\phi'' = \text{azimuth} + \text{backazimuth} - \phi$. This

84 simple geometric relationship is true for rays which are vertically incident at the surface,

4

but is only less accurate by a few degrees than a fully slowness-dependent expression, for the range of slownesses in this study. This error is generally less than the uncertainty in the method.

2.2. SKS UM splitting corrections

Seismic anisotropy in the continental UM (where our stations are located) appears to be ubiquitous, and is typically measured using phases such as SKS, PKS and SKKS; SKS is the most commonly used. It converts from a compressional to an S wave upon exiting the outer core, so begins its ascent through the mantle with no splitting present. It is polarised radially, hence it is also polarised parallel to the backazimuth at the receiver. SKS also propagates steeply through D″, which is known to be anisotropic in various places in the lower mantle (see reviews by Kendall and Silver, 1998, 2000; Lay et al., 1998; Nowacki et al., 2011). However, we assume that any contribution to splitting in the phase along this section is minor, as it has spent relatively little time in D″. Studies on a global scale support this approximation (Niu and Perez, 2004; Restivo and Helffrich, 2006), though any strong effects should be visible and display backazimuthal variation in splitting parameters (Hall et al., 2004).

Because we wish to remove UM anisotropy from the S phase, we choose seismic stations which have many SKS splitting measurements along a variety of backazimuths. If dipping or multiple layers of anisotropy exist beneath the station, then we expect the results to show a 90° or 180° periodicity to the measurements of ϕ and δt (Silver and Savage, 1994). We do not use stations which exhibit such measurements, as complicated UM anisotropy beneath the receiver is difficult to infer uniquely, and therefore we cannot confidently remove its effects on direct S phases, as they will be arbitrarily polarised compared to the backazimuth, depending on the source mechanism and anisotropic fabric they have encountered near the source. Stations which exhibit backazimuthal variation in SKS splitting may also do so because of laterally heterogeneous anisotropy beneath them. We also avoid using such stations for similar reasons. Our approach is slightly different from some authors, who opt to use stations which appear to show no anisotropy beneath them (Foley and Long, 2011),

5

however these are rare and UM anisotropy appears to be the norm, rather than isotropy.

Some studies using surface waves (e.g., Gaherty, 2004) or combining long-period waves with SKS splitting measurements (Yuan and Romanowicz, 2010) show evidence for multiple layers of anisotropy beneath North America, including beneath stations which do not exhibit backazimuthal variation in SKS splitting. It is possible that the same might also be true beneath Ethiopia. It therefore may be that any complexity of anisotropy (e.g., multiple layers) is not imaged in backazimuthal variations in splitting in SKS alone at our stations, despite the apparent requirement for it in surface waves, thus breaking the assumption of simple sub-station anisotropy. However, because our study is concerned only with shear wave splitting, so long as the splitting experienced by SKS and S is similar enough, this should not impact on the use of SKS splitting measurements as corrections here. The similarity between splitting in SKS and S for a given anisotropy beneath the seismic stations used here is therefore the critical assumption we make in this study.

In order to be confident of our measurements, we wish to make several for each MOR event, and so we choose from sets of stations in North America and Ethiopia, where extensive SKS splitting studies have been conducted (Ayele et al., 2004; Barruol et al., 1997; Evans et al., 2006; Fouch et al., 2000; Kendall et al., 2005; Liu, 2009; Niu and Perez, 2004; J.O.S. Hammond, pers. comm., 2010). As explained, we reject stations with apparently complicated sub-station anisotropy. SKS measurements for two example stations used in this study are shown in Supplementary Figure 1. The stations used in this study and the SKS splitting parameters used as UM corrections are shown in Supplementary Figure 2.

We use these SKS-derived corrections and analyse the direct S phase from events beneath MORs, applying the correction during the analysis. We note that even though reciprocity must apply along the ray path (see, for example, Kendall et al., 1992), the splitting operators are not commutative (Wolfe and Silver, 1998), so it is essential to make the corrections in the correct order (see Wookey and Kendall, 2008; Wookey et al., 2005). As a further check that the correction is valid, after the measurement we check that the source polarisation of S matches that predicted by the event's focal mechanism (see section 2.4). This helps mitigate against the possibility that the S phase we analyse is contaminated by depth phases (sS and

pS), as these will generally alter the apparent source polarisation of the combined phase to be different to that expected from the CMT solution. A difference in the measured source polarisation may also occur due to the application of an incorrect receiver correction in the analysis (see below), which also leads us to reject measurements where the two are not in agreement within 15°.

2.3. Testing the use of receiver corrections

Whilst we make every effort to ensure that we use seismic stations which have very well-characterised anisotropy beneath them, some error will be present in the measurement. Part of the difference will result because of the different slownesses between the S waves we study and the SKS phases used to make the splitting measurements we use as station corrections, but the difference is usually negligible in ϕ and very small in δt (see discussion in Nowacki et al., 2011). The majority of the error therefore likely comes from the assumption that the anisotropy is simple beneath the station, and that the SKS splitting measurements are accurate.

We conduct synthetic tests to determine how large the uncertainty in the measured source splitting parameters are when an 'incorrect' receiver correction is used. We apply a known initial amount of splitting (the 'source-side' splitting, $\phi_s''^{\mathrm{true}}, \delta t_s^{\mathrm{true}}$) to a synthetic wave of dominant frequency 0.1 Hz, then a known receiver-side splitting, $\phi_r^{\mathrm{true}}, \delta t_r^{\mathrm{true}}$. We then analyse the splitting in the wave with a range of receiver corrections ($\phi_r^{\mathrm{trial}}, \delta t_r^{\mathrm{trial}}$) to obtain the 'observed' splitting parameters at the source ($\phi_s''^{\mathrm{trial}}, \delta t_s^{\mathrm{trial}}$) and compare the known and measured source-side splitting. The procedure can be repeated for any combination of true source and receiver splitting operators, and all receiver 'corrections'.

Supplementary Figure 3 shows the difference between the true and measured splitting parameters where $\phi_s''^{\mathrm{true}} = 20°$, $\delta t_s^{\mathrm{true}} = 1.0\,\mathrm{s}$, and $\phi_r^{\mathrm{true}} = 0°$, $\delta t_r^{\mathrm{true}} = 1.0\,\mathrm{s}$. The difference in fast orientation, $\Delta(\phi'') = \mathrm{abs}(\phi_s''^{\mathrm{trial}} - \phi_s''^{\mathrm{true}})$, is within about 15° whilst the trial receiver correction is within about 40° and 0.4 s of the true receiver splitting parameters. In these limits, the difference in source delay time, $\Delta(\delta t) = \mathrm{abs}(\delta t_s^{\mathrm{trial}} - \delta t_s^{\mathrm{true}})$, is up to 0.6 s. Consistent with previous tests using real data (Russo and Mocanu, 2009), we find that errors in δt_r

7

appear to cause the largest uncertainty in the 'observed' source-side splitting parameters. Supplementary Figure 4 shows the case when $\phi_s''^{\text{true}} = 45°$, $\delta t_s^{\text{true}} = 1.0\,\text{s}$.

We also show in Supplementary Figures 3 and 4 the difference between the known and measured source polarisation for a range of ϕ_r^{trial} and $\delta t_r^{\text{trial}}$. The initial polarisation is 0° in both cases. Again, the difference in the true and trial receiver delay times plays a large rôle, and when the 'observed' source-side splitting parameters are most inaccurate, the source polarisation is often incorrect by about 10–20°. Hence the use of the source polarisation as a diagnostic of the quality of the result is important and helpful.

Finally, manual inspection of the results indicates that in several instances the 'observed' source splitting parameters would be classified as null events, especially where the delay times are large as shown in Supplementary Figures 3 and 4. This also highlights the strength of using manual inspection or an automated null-classifying scheme to maintain the integrity of measurements (Wuestefeld et al., 2010). When all of these diagnostics are included, and the receiver corrections are within an acceptable uncertainty range of within about 20° for the fast direction and 0.4 s for the delay time, we can be confident that the source-side shear wave splitting measurement is a true reflection of the splitting which has affected the wave in the source anisotropic region.

2.4. Event locations and focal mechanisms

In order to make inferences about anisotropy beneath MORs, it is obviously important to accurately know the earthquake location. Because MOR events typically have large uncertainties on their locations in time and space, where possible (for events before 2008) we take these parameters from the ISC's relocations using the EHB algorithm (Engdahl et al., 1998). The published horizontal uncertainty in the standard ISC locations is approximately 20 km; for the EHB locations in this study, the average uncertainty is 7 km.

The location of an event—whether beneath a ridge segment or transform zone—may affect the type of anisotropy we expect, hence each event was assigned to one of these categories based on its location relative to the bathymetry (Smith and Sandwell, 1997), and in part its focal mechanism. These were taken from the Global CMT catalogue. Where

8

there was ambiguity from bathymetry, the event was classified as being located on a ridge if the focal mechanism was mainly dip-slip, and as on a transform if mainly strike-slip.

2.5. Dataset

We consider events of $M > 5.0$, depth ≤ 35 km, in the epicentral distance range $55° \leq \Delta \leq 82°$, which are located on the East Pacific Rise (EPR), Mid-Atlantic Ridge (MAR), Gakkel Ridge, and the Southwest and Southeast Indian Ridges (IRs) (Figure 1). At distances less than $\sim 55°$, the difference in incidence angle between SKS and S becomes large enough that the vertical-incidence approximation may no longer be appropriate, and increases the possibility that an SKS-correction for UM anisotropy is inaccurate; beyond $\sim 82°$, the S phase interferes with ScS, or there may be a triplication due to the presence of the D″ layer, contaminating the S signal in the splitting analysis. We of course also wish to avoid D″-traversing rays due to the anisotropy present there. Events deeper than 35 km are unlikely to occur near MORs, and such depths may indicate a poor event location. The seismograms were band-pass filtered between 0.001 and 0.3 Hz.

After selection, over 2000 events matched the criteria between 1979 and 2009, according to the USGS National Earthquake Information Center (NEIC) and International Seismological Centre (ISC) catalogues. Due mainly to signal-to-noise requirements, ~ 400 events were retained for analysis, leaving ~ 820 event-station pairs.

During analysis, we apply a strict set of criteria to select the optimum splitting results. Only non-null results which meet the following are retained: (i) acceptable signal-to-noise ratio on both horizontal components; (ii) clear elliptical particle motion before analysis; (iii) clear linearisation of particle motion when corrected; (iv) measured source polarisation is within 15° of the CMT-predicted source polarisation; (v) clear minimum on the λ_2 surface. A quality of 1 (excellent) to 4 (very poor) is assigned manually to each measurement. Null measurements are retained, provided the signal-to-noise ratio is adequate and particle motion is clearly linear before analysis, but after correction for receiver anisotropy.

Following analysis, 350 measurements of splitting of 'fair' (3) quality or better beneath 67 events comprise the dataset. Of these, 122 are of quality 'good' (2) or better. There are

9

189 null measurements. The events have magnitude range $4.4 \leq M_b \leq 6.7$, and depth range 0–33 km.

3. Results

3.1. East Pacific Rise

The EPR is the best-sampled MOR segment in this work. Our results agree excellently with SKS splitting results from ocean-bottom seismometers (OBSs) deployed as part of the MELT and GLIMPSE projects (Wolfe and Solomon, 1998; Harmon et al., 2004) (orange bars, Figure 2). Here and in the OBS experiments, ϕ'' or ϕ_{SKS} is approximately parallel to the spreading direction, with δt varying from 1–3 s, depending on distance from the ridge axis. Figure 3 shows the variation of splitting parameters with distance for results on the EPR which are classified as 'ridge' events, alongside the MELT and GLIMPSE data.

Away from the straightest segments of the EPR, where frequent fracture zones offset the ridge axis, the pattern of observed splitting is different. There is no clear spreading direction-parallel trend to ϕ'', and the change in δt is also complicated. At about $-5°$ latitude, for example, ϕ'' seems to change over a short distance by $\sim 70°$ from spreading direction-parallel to transform zone-perpendicular. Similarly, the pattern of ϕ'' and δt east of the Pacific–Nazca–Antarctic triple-junction is also complex, with a variation of ϕ'' from parallel to perpendicular to the Challenger Fracture Zone (at about $-35°$ latitude).

3.2. Mid-Atlantic Ridge

Events which produced 'good' source-side splitting measurements were limited to latitudes between $-40°$ and $15°$. Very few events of sufficient magnitude are reported in the catalogues along the Reykjanes Ridge, and no 'good' measurements could be made north of the equator. We note that few measured earthquakes occur along clear, linear ridge segments along the MAR, and most seismicity for which we have results is located instead on the transform zones. Nonetheless, the few events clearly beneath ridges (e.g., the stack at $-30°$ latitude) do seem to show spreading direction-parallel ϕ''. This agrees approximately

10

with SKS splitting measurements made at ASCN (Butt Crater, Ascension Island; Wolfe and Silver, 1998) and SHEL (Horse Pasture, St. Helena; Behn et al., 2004).

Along transform zones, about half the results show ϕ'' close to the spreading direction, whilst many show large ($\sim$2.5–3 s) δt and ϕ'' roughly perpendicular to the strike of the transform. The dependence of splitting parameters upon distance along the transform zone, away from the nearest ridge segment, is shown in Supplementary Figure 5. The pattern shows considerable variation near the ends of the transform zones, close to the ridge axes, perhaps related to the complex tectonic environment and resultant shearing and melt production. However, there is a decrease in the maximum delay time as distance from the ridge axis increases, possibly indicating a reduced contribution from a mechanism of anisotropy arising due to melt or other sub-axial process.

Two events on the MAR gave results at stations in both North America and Ethiopia. In this case, we may examine the azimuthal dependence of the splitting. Figure 5 shows equal-area lower-hemisphere stereoplots of the splitting parameters, which are notably different along the two different azimuths. Splitting measured at North American stations for both events has smaller δt (stacked splitting parameters: $\phi'' = (25\pm4)°$, $\delta t = (1.9\pm0.1)\,\text{s}$), whereas δt is larger when measured along the other azimuth at Ethiopian stations ($\phi'' = (76 \pm 2)°$, $\delta t = (2.6 \pm 0.1)\,\text{s}$). At this limited range of slownesses, there is not much variation in the angle away from the vertical for the rays, so the differences primarily arise due to azimuth. The Fresnel zones of the two rays of period 20 s stop overlapping significantly when deeper than $\sim$200 km, so if heterogeneity were the cause, then the majority of the anisotropy would need to be present below this.

3.3. Gakkel Ridge

Ten results from events on the Gakkel Ridge were of 'good' or better quality, with an equal number of null results. The splitting parameters are shown in Figure 6A. It is notable that most results show a small amount of splitting ($\langle\delta t\rangle = 1.1$ s), and there is a higher proportion of null results than in other regions. The splitting that is present is often ridge-parallel. The spreading rate predicted by NUVEL-1A (DeMets et al., 1994) increases from

11

$_{280}$ ∼6 to 18 mm a^{-1} from right to left in Figure 6A, however there is no clear corresponding

$_{281}$ trend in the amount of splitting. There is also no obvious systematic variation of parameters

$_{282}$ for the cluster of events furthest north (rightmost in Figure 6A, circled) with azimuth. A

$_{283}$ lower amount of splitting beneath such extremely slow-spreading ridges might be related to

$_{284}$ reduced melt production caused by slow exhumation of material and a consequently small

$_{285}$ amount of adiabatic decompression melting. If this is the case, the dominant contribution

$_{286}$ to seismic anisotropy at teleseismic distances would then be from LPO, yet the axis-parallel

$_{287}$ fast orientations we observe are hard to explain via mineral alignment.

$_{288}$ *3.4. Southwest and Southeast Indian Ridges*

$_{289}$ Beneath events on the SWIR and SEIR, 43 individual results, allowing three stacked

$_{290}$ results, and seven null measurements were made. These are shown in Figure 6B. Again, the

$_{291}$ pattern is complicated, and few events lie on ridge segments: most are on transforms. The

$_{292}$ Southwest Indian Ridge shows some of the most oblique spreading of any MOR, so it may

$_{293}$ help distinguish between processes which lead to anisotropy which is ridge-perpendicular

$_{294}$ or spreading direction parallel. However, there are insufficient large earthquakes to make

$_{295}$ any strong inferences from source-side splitting. Interestingly, all measurements made from

$_{296}$ beneath the ridge segment at longitude 20° appear to be null. This might result from the

$_{297}$ absence of anisotropy in the region, but it may also occur if the source polarisation is parallel

$_{298}$ or perpendicular the local fast orientation of some anisotropy. With only one azimuth of

$_{299}$ measurements and no other events with different source polarisations, it is not possible to

$_{300}$ distinguish these scenarios.

$_{301}$ **4. Interpretation and discussion**

$_{302}$ In interpreting our results, it is difficult to draw firm conclusions about the behaviour of

$_{303}$ MORs in general because of poor sampling, arising from the lack of stations outside USA

$_{304}$ and Ethiopia with comprehensive studies published on the backazimuthal variation of SKS

$_{305}$ splitting parameters. For the purposes of studying relatively small-magnitude earthquakes

$_{306}$ at teleseismic distances such as is done here, networks of stations with such measurements

are necessary to allow stacking of data, especially when fast directions are near the source polarisation. This limitation also means that comparisons between fast and slow ridges are hard to make. However, our measurements do suggest that splitting near the ridge axis is greater beneath fast-spreading ridges (full-rate $> 100 \text{ mm a}^{-1}$) than slow-spreading ones.

Our measurements of splitting show ϕ'' to be very similar to the fast orientations observed by regional SKS studies near MORs, but these are extremely limited in coverage because of the practical difficulties in operating such OBS sites. Surface wave studies examining azimuthal anisotropy globally (e.g., Debayle et al., 2005) can provide better coverage near MORs, but limited horizontal resolution means changes over relatively small distances (up to few tens of kilometres and less) cannot be imaged well. Such global measurements tend to show fast orientations approximately parallel to the spreading direction, but this can vary by up to 45° in some places, notably near large fracture zones.

4.1. Doldrums FZ observations

The multi-azimuth observations beneath the Doldrums Fracture Zone (FZ) in section 3.2 are interesting (Figure 5). The observation of this azimuthal dependence in splitting parameters appears to be a robust feature: tests requiring ϕ'' to be the same for stations in Ethiopia and North America show the splitting experienced by the direct S wave beneath both sets of stations would have to be different by around 45° to that observed in SKS waves and for which we correct. Such a strong incidence dependence in splitting beneath the receiver would in all likelihood appear as complexity in SKS splitting observations, and here we deliberately avoid stations where this is the case. Whilst the limited number of data prevents detailed analysis, we can speculate on the likely causes of the observed pattern.

With two azimuths of observations, we can seek to define an hexagonal symmetry, oriented arbitrarily (called 'tilted transverse isotropy', or TTI). If we assume Thomsen's (1986) anisotropic parameters $\delta = \epsilon$ (the case of elliptical anisotropy), we can use the two azimuths of observations to find the plane of isotropy, or axis of symmetry, by simple trigonometry (Nowacki et al., 2011). This dips shallowly to the southwest, as shown by the dashed line in Figure 7. For TTI derived from aligned material, for instance, this would correspond to

13

penny-shaped inclusions having their short axis aligned about 35° from the vertical. This is in some sense similar to the orientations predicted by simulations (Weatherley and Katz, 2010), which suggest melt should be focussed along northwest–southeast flow lines for a transform in this orientation. Intriguingly, it also would be consistent with the suggestion of van Wijk and Blackman (2005), who speculate that the transform fault itself would dip towards the ridge segment near the ends of the transform.

Another likely contributor to seismic anisotropy in the FZ would be the alignment of olivine in response to flow. Natural samples and deformation experiments show that the dominant way in which olivine develops an LPO is by slip along [100] (a-direction), on {0kl} or (010) (b-planes), known as D- and A-type olivine respectively. We examine the possibility that the observed anisotropy at the Doldrums FZ is caused by olivine LPO by using the method described by Wookey and Kendall (2008) and Nowacki et al. (2010). We use the single-crystal elastic constants of olivine (Abramson et al., 1997) and mix them in all proportions with an isotropic average. We then rotate these constants to all possible orientations and compute the shear wave splitting accrued over a 200 km thick layer for the two raypaths observed, and plot the orientations producing splitting compatible with the observations. Figure 7 shows the compatible orientations and degree of alignment as the a- and b-axes of the aligned olivine on a lower-hemisphere equal-area projection.

Compatible orientations of the a-axes are northwest–southeast, with glide planes dipping north, northwest or west, all shallowly. This direction of shear is not parallel to the spreading direction or FZ strike, or to the absolute plate motion (APM) (Figure 4). It is consistent with some dynamics models of ridge transforms (e.g., van Wijk and Blackman, 2005; Sparks et al., 1993; Phipps Morgan and Forsyth, 1988), though such models also predict low strain rates in such regions and relate to shorter FZs. This interpretation is, however, inconsistent with the expected behaviour for a pure strike-slip fault, where strains are sufficiently high that olivine [100] directions should be parallel to the FZ strike. This incongruity might support the hypothesis that SPO due to melt or another material is the cause: if olivine [100] directions were parallel with APM or FZ strike, but some other anisotropy were overprinted, then we would not necessarily retrieve the olivine orientations with this method. Equally,

14

such conditions as are present beneath the FZ might lead to the dominance of a different slip system in olivine, in which case flow might still be parallel to the FZ, but not olivine [100] axes. Whilst the uncertainty in our measurements is not insignificant, even with more relaxed constraints on the orientations the picture is much the same (Supplementary Figure 6). We of course neglect other anisotropic phases in this approach, but would expect this to require a stronger texturing in the olivine itself to match observations.

Finally, heterogeneity between the two raypaths away from the source may also be important, as paths to Ethiopia spend considerable distance close to the FZ, whilst paths to North America travel away from this region. This would have to be true at depths of ∼200 km, as the Fresnel zones of waves of this period overlap significantly until that depth. Hence the signal may reflect different anisotropies along these two paths, perhaps with the addition of a common anisotropic region immediately below the source. However, other studies (e.g.,) suggest that such strong anisotropy at depths is unlikely, and we prefer to interpret the observations in terms of a mixture of olivine alignment and SPO

4.2. Spreading rate and strength of anisotropy

Dynamic models of MOR accretion have predicted the amount and orientation of shear wave splitting near spreading ridges on the basis of LPO of pure olivine (Blackman et al., 1996), LPO of olivine and enstatite (Blackman et al., 2002; Blackman and Kendall, 2002; Nippress et al., 2007), and combined olivine LPO with the effect of oriented melt pockets (Blackman and Kendall, 1997). In such models, the spreading rate controls the behaviour of upwelling beneath the ridge axis and the shape of the melt-rich region, and hence the orientation and amount of shear wave splitting observed at the surface. In Blackman and Kendall's (2002) simulations, slow spreading ridges (full-rate ∼40 mm a^{-1}) show significant ridge-parallel splitting within ∼20 km from the axis because of the requirement that buoyant flow beneath the ridge axis supplies the upwelling material in a small region. Fast-spreading (full-rate ∼140 mm a^{-1}) ridges, by contrast, do not focus material so efficiently towards the centre and should not produce much observable difference in splitting times between the ridge axis and at distance (> 50 km). Both cases show ∼0.5–1 s of splitting away from

15

the axis. Hence their model predicts there should be little observable difference in splitting in SKS for fast ridges at the axis compared to at distance (>50 km). This agrees with SKS measurements at the EPR (Wolfe and Solomon, 1998; Harmon et al., 2004), where full-spreading rates are >60 mm a^{-1}, and on average ~150 mm a^{-1}.

Figure 8 shows δt versus spreading rate for measurements made beneath ridge events, with filled circles indicating those within 50 km of the ridge axis. The above models would predict a negative trend in the near-axis data, with larger splitting times observed at the slowest spreading centres; however, there is no strong trend apparent in our results and the data suggest a weakly positive correlation if any. (Weighted least-squares linear regression for results <50 km from axis gives $R^2 = 0.42$.)

Whilst most authors predict increased splitting at the slowest MORs, some observations suggest that anisotropy away from the ridge increases with palaeo-spreading rate. P wave anisotropy in the shallow lithosphere beneath the northwest Atlantic (spreading full-rate ~20 mm a^{-1}) is significantly less at ~3 % (Gaherty et al., 2004) than that observed at present-day fast-spreading sites near the East Pacific Rise (~6 %, rate ~100 mm a^{-1}) (Dunn and Toomey, 1997) and old lithosphere in the western Pacific (~6 %, palaeo-rate ~60 mm a^{-1}) (Shearer and Orcutt, 1986). Such observations constrain the anisotropy in the uppermost mantle, hence probably reflect the effect of 'frozen-in' olivine LPO and processes contemporaneous with lithosphere creation. Gaherty et al. (2004) suggest a spreading rate dependence could be due to slower ridges accommodating more deformation by brittle failure in the crust, leading to reduced LPO in the uppermost mantle. However, our shear wave splitting measurements integrate anisotropy over the complete ray path in the upper mantle, and it is not clear that this effect could cause the change in δt we observe, given the thickness of the brittle crust.

It is also important to note that this discussion ignores any azimuthal dependence on splitting parameters. With stations only in North America and Ethiopia, there may be an azimuthal bias between ridges of different spreading rates, which could account for some of the variability we observe.

16

4.3. Splitting in S and SKS at the EPR

Figure 3 indicates that the amount of shear wave splitting in direct S increases away from the ridge more quickly than that in SKS phases. Assuming that the splitting is accrued over a horizontal layer of constant anisotropy, this difference cannot be accounted for simply by the difference in incidence angle between the phases (which would predict a difference in δt of $\lesssim 0.3\,\text{s}$ for the largest δt_{SKS}). Accruing splitting operators through a model of LPO development at the EPR (Blackman and Kendall, 2002) along the raypaths of the S and SKS phases also indicates that the contrasting azimuths and incidences of the waves are insufficient to produce the observed discrepancy.

One possible explanation might be along-ridge variability in the strength and style of mantle anisotropy, leading to varying splitting dependent on the location along ridge segments. This would imply a sampling bias, whereby events nearest the ridge are in weak anisotropy regions, whilst those furthest are in strong anisotropy regions. This correlation arising by chance or through some earthquake mechanism seems unlikely. More likely may be the influence of azimuth and large-scale heterogeneity. SKS waves travelling to the MELT and GLIMPSE OBSs are along a backazimuth of $\sim 280°$, approximately ridge-perpendicular, whilst S waves in this study travel along an azimuth of $\sim 20°$, closely parallel to the ridge. Hence the S waves may be more sensitive to ridge structure for events near the ridge, and less so at distance, magnifying the contrast in structure between the on- and off-axis mantle.

Another simple explanation may be that current LPO models do not include effects of short-wavelength segregation of material such as that observed in experiments which deform partially molten olivine aggregates (Holtzman et al., 2003a,b), and in numerical experiments incorporating porosity and strain rate-dependent viscosity (Katz et al., 2006). These observations predict lenses of melt at MORs will be aligned approximately with long axes of the strain ellipses expected for corner flow, forming bands which dip away from the ridge axis, becoming approximately horizontal beyond about $50\,\text{km}$ from the centre. The alignment of seismically distinct material on scales shorter than the seismic wavelength would lead to a shape-preferred orientation (SPO). Such an SPO with inclusions of uniaxial symmetry would lead to transverse isotropy (TI), where the seismic velocities and amount

of splitting vary only away from the axis of rotational symmetry (e.g., Hudson, 1980). This would mean SKS waves travelling perpendicular to the axis (such as those measured by the MELT and GLIMPSE OBSs) would not be split due being polarised in the sagittal plane, whilst near the ridge fast orientations for S waves would be between ridge-parallel and ridge-perpendicular, depending on the dip of the fabric. Further from the ridge, where bands are horizontal, SKS would be unsplit in any azimuth; S waves travelling parallel to the ridge would have ridge-perpendicular fast orientations. This mechanism would increase delay times in S over SKS away from the axis, as we observe at the EPR. Aligned inclusions leading to SPO could also explain surface wave observations that $V_{SH} > V_{SV}$ beneath the Pacific (e.g., Ekström and Dziewoński, 1998; Nettles and Dziewoński, 2008), and receiver function observations of a suboceanic seismic discontinuity at depths of 50 to 150 km (the so-called 'LAB' discontinuity; Rychert and Shearer, 2009; Kawakatsu et al., 2009; Rychert et al., 2010; Kumar and Kawakatsu, 2011).

Several studies show that the structure beneath the EPR is asymmetric (e.g., Conder, 2007; Harmon et al., 2004; Podolefsky et al., 2004; Wolfe and Solomon, 1998), hence this might play some part in the observed difference in splitting times between S and SKS phases. However, our data also sample both sides of the ridge, so presumably are also affected by the same asymmetry, yet still consistently show larger splitting in S than SKS. Blackman and Kendall (1997) calculate the splitting times for vertical-incidence shear waves on a suite of asymmetric model of MOR LPO development, as for the EPR, and for the best-fitting case predict splitting times for SKS of up to 2–3 s on the Pacific plate, and up to 1.5 s on the Nazca plate. This asymmetry is observed to a lesser extent in the data (Figure 3). However, again the effect of azimuth is not tested and the path of the S waves (ridge-parallel) may negate some of the effects on δt expected for an asymmetric spreading centre.

4.4. Plate motion and mantle flow

Several authors interpret shear wave splitting measurements in terms of the alignment of olivine due to shearing of the asthenosphere by the relative motion of the lithosphere above it (e.g., Tommasi, 1998; Conrad et al., 2007). In this study, it is hard to discriminate

18

between this and spreading processes for the EPR, MAR and SWIR because the directions of spreading and APM are very similar (Figures 2, 4 and 6). APM is also small (<10 mm a^{-1}) at the SWIR. Beneath our measurements on the SEIR, the APM is eastwards, but no fast orientations are parallel to this. At the eastern Gakkel ridge, plate motion is approximately parallel to the ridge, and is faster than the spreading rate ($|\text{APM}| \approx 12$ mm a^{-1}). It may be, therefore, that the ridge-parallel ϕ'' reflects the shearing of the North American and Eurasian plates over the asthenosphere. Another interpretation would be that because spreading rate varies along the ridge, mantle material again flows parallel to the axis, again leading to olivine LPO with [100] directions which are compatible with our observations. In both cases, however, the mechanisms which cause this at spreading centres themselves is still unclear. Conrad et al. (2007) point out that parallelism between APM direction and olivine a-axes—assuming LPO in olivine to be the cause of the observed anisotropy—may not be a good assumption beneath MORs, because of the complicated combination of radial and horizontal flow present there. One might also expect along-axis flow of material due to the fact that spreading rate varies along the ridge, which might also explain ridge-parallel fast orientations.

A more involved explanation of upper mantle shear wave splitting results can be invoked by considering more complex flow regimes. Behn et al. (2004), for instance, combine plate motion models with a model of mantle flow derived from seismic tomography, and compare SKS splitting observations with the fast orientations predicted by the flow models. In this case, the authors conclude that plate spreading directions adequately describe SKS fast orientations on oceanic plates within 500 km of the ridge. In this study, only one measurement is further than this from the spreading centre (westernmost stack in Figure 2), and here the fossil spreading direction and APM are the same within a few degrees. This might serve to reinforce the fossil anisotropy in the lithosphere, but δt here is modest ($(1.7 \pm 0.5)\,$s).

Where inferred mantle flow beneath Africa might affect our measurements, on the SWIR, we see several fast orientations parallel to the spreading direction, however one stacked measurement (Figure 6) at $\sim32°$E is perpendicular to spreading. This direction does not

19

correlate with APM. Whilst more rigorous modelling of deeper flow could be attempted (e.g., Forte et al., 2010), this is beyond the scope of this study, and may be more appropriate when further data are presented.

5. Conclusions

We present measurements made using the source-side shear wave splitting technique of upper mantle anisotropy beneath mid-ocean ridges around the world. We correct for the UM on the receiver side for seismic stations where the anisotropy beneath is very well characterised, and can resolve the source anisotropy, subject to a series of rigorous tests. With 122 new observations, the presented dataset adds significantly to the current knowledge of anisotropy beneath MORs. There is no strong trend that corroborates the prediction of more splitting beneath slow-spreading ridges, and it may be true that more splitting is present at fast-spreading ones. For the EPR, comparisons with previous SKS splitting measurements show more splitting in S away from the ridge. We suggest that TI dipping away from the ridge axis, becoming horizontal at distance, is compatible with our observations, in addition to LPO development. This would be consistent with other observations of anisotropy and a seismic discontinuity beneath the oceans. We find anisotropy at MORs appears to be dominated by ridge processes, rather than plate motion over the asthenosphere. As further rigorous study of UM anisotropy using SKS phases becomes routine, more stations can be used to measure the seismic shear wave splitting beneath MORs and other remote parts of the Earth where earthquakes occur, and hence our understanding of mantle dynamics in these regions will be vastly improved.

6. Acknowledgements

20

References

Abramson, E., Brown, J., Slutsky, L., Zaug, J., 1997. The elastic constants of San Carlos olivine to 17 GPa. J Geophys Res-Sol Ea 102 (B6), 12253–12263.

Ayele, A., Stuart, G., Kendall, J. M., 2004. Insights into rifting from shear wave splitting and receiver functions: an example from Ethiopia. Geophys J Int 157 (1), 354–362.

Barclay, A., Toomey, D., 2003. Shear wave splitting and crustal anisotropy at the Mid-Atlantic Ridge, 35° N. J Geophys Res-Sol Ea 108 (B8), 2378.

Barruol, G., Helffrich, G., Vauchez, A., 1997. Shear wave splitting around the northern Atlantic: frozen Pangaean lithospheric anisotropy? Tectonophysics 279 (1-4), 135–148.

Becker, T. W., Ekström, G., Boschi, L., Woodhouse, J. H., 2007. Length scales, patterns and origin of azimuthal seismic anisotropy in the upper mantle as mapped by Rayleigh waves. Geophys J Int 171 (1), 451–462.

Behn, M., Conrad, C., Silver, P. G., 2004. Detection of upper mantle flow associated with the African Superplume. Earth Planet Sci Lett 224 (3-4), 259–274.

Bird, P., 2003. An updated digital model of plate boundaries. Geochem Geophy Geosy 4, 1027.

Blackman, D., Kendall, J. M., 1997. Sensitivity of teleseismic body waves to mineral texture and melt in the mantle beneath a mid-ocean ridge. Philos T R Soc A 355 (1723), 217–231.

Blackman, D., Kendall, J. M., 2002. Seismic anisotropy in the upper mantle 2. Predictions for current plate boundary flow models. Geochem Geophy Geosy 3, 8602.

Blackman, D., Kendall, J. M., Dawson, P., Wenk, H.-R., Boyce, D., Phipps Morgan, J., 1996. Teleseismic imaging of subaxial flow at mid-ocean ridges: Traveltime effects of anisotropic mineral texture in the mantle. Geophys J Int 127 (2), 415–426.

Blackman, D., Orcutt, J., Forsyth, D., 1995a. Recording teleseismic earthquakes using ocean-bottom seismographs at mid-ocean ridges. B Seismol Soc Am 85 (6), 1648–1664.

Blackman, D., Orcutt, J., Forsyth, D., Kendall, J. M., 1993. Seismic anisotropy in the mantle beneath an oceanic spreading center. Nature 366 (6456), 675–677.

Blackman, D., Orcutt, J., Forsyth, D., Kendall, J. M., 1995b. Correction to: 'Seismic anisotropy in the mantle beneath an oceanic spreading center (vol 366, pg 675, 1993)'. Nature 374 (6525), 824–824.

Blackman, D., Wenk, H.-R., Kendall, J. M., 2002. Seismic anisotropy of the upper mantle 1. Factors that affect mineral texture and effective elastic properties. Geochem Geophy Geosy 3, 8601.

Conder, J. A., 2007. Dynamically driven mantle flow and shear wave splitting asymmetry across the EPR, MELT area. Geophys Res Lett 34 (16), L16301.

Conrad, C. P., Behn, M. D., Silver, P. G., 2007. Global mantle flow and the development of seismic anisotropy: Differences between the oceanic and continental upper mantle. J Geophys Res-Sol Ea

112 (B7), B07317.

Debayle, E., Kennett, B., Priestley, K., 2005. Global azimuthal seismic anisotropy and the unique plate-motion deformation of Australia. Nature 433 (7025), 509–512.

Delorey, A. A., Dunn, R. A., Gaherty, J. B., 2007. Surface wave tomography of the upper mantle beneath the Reykjanes Ridge with implications for ridge-hot spot interaction. J Geophys Res-Sol Ea 112 (B8), B08313.

DeMets, C., Gordon, R. G., Argus, D. F., Stein, S., 1994. Effect of recent revisions to the geomagnetic reversal time scale on estimates of current plate motions. Geophys Res Lett 21 (20), 2191–2194.

Dunn, R., Toomey, D., 1997. Seismological evidence for three-dimensional melt migration beneath the East Pacific Rise. Nature 388 (6639), 259–262.

Ekström, G., Dziewoński, A., 1998. The unique anisotropy of the pacific upper mantle. Nature 394 (6689), 168–172.

Engdahl, E., van der Hilst, R. D., Buland, R., 1998. Global teleseismic earthquake relocation with improved travel times and procedures for depth determination. B Seismol Soc Am 88 (3), 722–743.

Evans, M., Kendall, J. M., Willemann, R., 2006. Automated SKS splitting and upper-mantle anisotropy beneath Canadian seismic stations. Geophys J Int 165 (3), 931–942.

Ferreira, A. M. G., Woodhouse, J. H., Visser, K., Trampert, J., 2010. On the robustness of global radially anisotropic surface wave tomography. J Geophys Res-Sol Ea 115, B04313.

Foley, B. J., Long, M. D., 2011. Upper and mid-mantle anisotropy beneath the Tonga slab. Geophys Res Lett 38 (2), L02303.

Forte, A. M., Quere, S., Moucha, R., Simmons, N. A., Grand, S. P., Mitrovica, J. X., Rowley, D. B., 2010. Joint seismic-geodynamic-mineral physical modelling of african geodynamics: A reconciliation of deep-mantle convection with surface geophysical constraints. Earth Planet Sci Lett 295 (3-4), 329–341.

Fouch, M. J., Fischer, K. M., Parmentier, E., Wysession, M., Clarke, T., 2000. Shear wave splitting, continental keels, and patterns of mantle flow. J Geophys Res-Sol Ea 105 (B3), 6255–6275.

Gaherty, J., 2004. A surface wave analysis of seismic anisotropy beneath eastern North America. Geophys J Int 158 (3), 1053–1066.

Gaherty, J., Lizarralde, D., Collins, J., Hirth, G., Kim, S., 2004. Mantle defomation during slow seafloor spreading constrained bv observations of seismic anisotropy in the western Atlantic. Earth Planet Sci Lett 228 (3-4), 255–265.

Gaherty, J. B., 2001. Seismic evidence for hotspot-induced buoyant flow beneath the Reykjanes Ridge. Science 293 (5535), 1645–1647.

Gripp, A., Gordon, R., 2002. Young tracks of hotspots and current plate velocities. Geophys J Int 150 (2), 321–361.

600 Hall, S. A., Kendall, J. M., der Baan, M. V., 2004. Some comments on the effects of lower-mantle anisotropy
601   on SKS and SKKS phases. Phys. Earth Planet. Inter. 146 (3-4), 469–481.

602 Harmon, N., Forsyth, D., Fischer, K. M., Webb, S., 2004. Variations in shear-wave splitting in young Pacific
603   seafloor. Geophys Res Lett 31 (15), L15609.

604 Hess, H., 1964. Seismic anisotropy of uppermost mantle under oceans. Nature 203 (494), 629–&.

605 Holtzman, B. K., Groebner, N., Zimmerman, M., Ginsberg, S., Kohlstedt, D., 2003a. Stress-driven melt
606   segregation in partially molten rocks. Geochem Geophy Geosy 4, 8607.

607 Holtzman, B. K., Kendall, J. M., 2010. Organized melt, seismic anisotropy, and plate boundary lubrication.
608   Geochem Geophy Geosy 11, Q0AB06.

609 Holtzman, B. K., Kohlstedt, D., Zimmerman, M., Heidelbach, F., Hiraga, T., Hustoft, J. W., 2003b. Melt seg-
610   regation and strain partitioning: Implications for seismic anisotropy and mantle flow. Science 301 (5637),
611   1227–1230.

612 Hudson, J., 1980. Overall properties of a cracked solid. Math Proc Camb Phil Soc 88 (2), 371–384.

613 Hung, S., Forsyth, D., 1999. Anisotropy in the oceanic lithosphere from the study of local intraplate earth-
614   quakes on the west flank of the southern East Pacific Rise: Shear wave splitting and waveform modeling.
615   J Geophys Res-Sol Ea 104 (B5), 10695–10717.

616 Katz, R. F., Spiegelman, M., Holtzman, B., 2006. The dynamics of melt and shear localization in partially
617   molten aggregates. Nature 442 (7103), 676–679.

618 Kawakatsu, H., Kumar, P., Takei, Y., Shinohara, M., Kanazawa, T., Araki, E., Suyehiro, K., 2009. Seismic
619   evidence for sharp lithosphere-asthenosphere boundaries of oceanic plates. Science 324 (5926), 499–502.

620 Kendall, J. M., 1994. Teleseismic arrivals at a mid-ocean ridge: Effects of mantle melt and anisotropy.
621   Geophys Res Lett 21 (4), 301–304.

622 Kendall, J. M., Guest, W., Thomson, C., 1992. Ray-theory Green's function reciprocity and ray-centered
623   coordinates in anisotropic media. Geophys J Int 108 (1), 364–371.

624 Kendall, J.-M., Silver, P. G., 1998. Investigating causes of D″ anisotropy. In: Gurnis, M., Wysession, M. E.,
625   Knittle, E., Buffett, B. A. (Eds.), The Core–Mantle Boundary Region. Geodynamics Series. American
626   Geophysical Union, Washington, D.C., USA, pp. 97–118.

627 Kendall, J.-M., Silver, P. G., 2000. Seismic anisotropy in the boundary layers of the mantle. In: Karato, S.,
628   Forte, A., Liebermann, R. C., Masters, G., Stixrude, L. (Eds.), Earth's Deep Interior: Mineral Physics
629   and Tomography from the Atomic to the Global Scale. Vol. 117 of Geophysical Monograph. American
630   Geophysical Union, Washington, D.C., USA, pp. 133–159.

631 Kendall, J. M., Stuart, G., Ebinger, C., Bastow, I., Keir, D., 2005. Magma-assisted rifting in Ethiopia.
632   Nature 433 (7022), 146–148.

633 Kennett, B., Engdahl, E., 1991. Traveltimes for global earthquake location and phase identification. Geophys

23

J Int 105 (2), 429–465.

Kumar, P., Kawakatsu, H., 2011. Imaging the seismic lithosphere-asthenosphere boundary of the oceanic plate. Geochem Geophy Geosy 12 (1), Q01006.

Kustowski, B., Ekström, G., Dziewoński, A., 2008. Anisotropic shear-wave velocity structure of the Earth's mantle: A global model. J Geophys Res-Sol Ea 113 (B6), B06306.

Lay, T., Williams, Q., Garnero, E. J., Kellogg, L., Wysession, M. E., 1998. Seismic wave anisotropy in the D″ region and its implications. In: Gurnis, M., Wysession, M. E., Knittle, E., Buffett, B. A. (Eds.), The Core–Mantle Boundary Region. Geodynamics Series 28. American Geophysical Union, Washington, D.C., USA, pp. 299–318.

Liu, K. H., 2009. NA-SWS-1.1: A uniform database of teleseismic shear wave splitting measurements for North America. Geochem Geophy Geosy 10, Q05011.

Long, M. D., Silver, P. G., 2009. Shear wave splitting and mantle anisotropy: Measurements, interpretations, and new directions. Surv Geophys 30 (4-5), 407–461.

Mainprice, D., 2007. Seismic anisotropy of the deep earth from a mineral and rock physics perspective. In: Schubert, G. (Ed.), Treatise on Geophysics. Vol. 2. pp. 437–492.

Meade, C., Silver, P. G., Kaneshima, S., 1995. Laboratory and seismological observations of lower mantle isotropy. Geophys Res Lett 22 (10), 1293–1296.

Montagner, J.-P., Kennett, B., 1996. How to reconcile body-wave and normal-mode reference earth models. Geophys J Int 125 (1), 229–248.

Nettles, M., Dziewoński, A., 2008. Radially anisotropic shear velocity structure of the upper mantle globally and beneath North America. J Geophys Res-Sol Ea 113 (B2), B02303.

Nippress, S. E. J., Kusznir, N. J., Kendall, J. M., 2007. LPO predicted seismic anisotropy beneath a simple model of a mid-ocean ridge. Geophys Res Lett 34 (14), L14309.

Niu, F., Perez, A., 2004. Seismic anisotropy in the lower mantle: A comparison of waveform splitting of SKS and SKKS. Geophys Res Lett 31 (24), L24612.

Nowacki, A., Wookey, J., Kendall, J. M., 2010. Deformation of the lowermost mantle from seismic anisotropy. Nature 467 (7319), 1091–1095.

Nowacki, A., Wookey, J., Kendall, J.-M., 2011. New advances in using seismic anisotropy, mineral physics and geodynamics to understand deformation in the lowermost mantle. J Geod doi:10.1016/j.jog.2011.04.003.

Panning, M., Romanowicz, B., 2006. A three-dimensional radially anisotropic model of shear velocity in the whole mantle. Geophys J Int 167 (1), 361–379.

Phipps Morgan, J., 1987. Melt migration beneath mid-ocean spreading centers. Geophys Res Lett 14 (12), 1238–1241.

Phipps Morgan, J., Forsyth, D., 1988. Three-dimensional flow and temperature perturbations due to a

24

transform offset: effects on oceanic crustal and upper mantle structure. J Geophys Res-Solid 93 (B4), 2955–2966.

Podolefsky, N., Zhong, S., McNamara, A. K., 2004. The anisotropic and rheological structure of the oceanic upper mantle from a simple model of plate shear. Geophys J Int 158 (1), 287–296.

Restivo, A., Helffrich, G., 2006. Core-mantle boundary structure investigated using SKS and SKKS polarization anomalies. Geophys J Int 165 (1), 288–302.

Russo, R., Mocanu, V. I., 2009. Source-side shear wave splitting and upper mantle flow in the Romanian Carpathians and surroundings. Earth Planet Sci Lett 287 (1-2), 205–216.

Rychert, C. A., Shearer, P. M., 2009. A global view of the lithosphere-asthenosphere boundary. Science 324 (5926), 495–498.

Rychert, C. A., Shearer, P. M., Fischer, K. M., 2010. Scattered wave imaging of the lithosphere-asthenosphere boundary. Lithos 120 (1-2), 173–185.

Savage, M., 1999. Seismic anisotropy and mantle deformation: What have we learned from shear wave splitting? Rev. Geophys. 37 (1), 65–106.

Schoenecker, S., Russo, R., Silver, P., 1997. Source-side splitting of S waves from Hindu Kush-Pamir earthquakes. Tectonophysics 279 (1-4), 149–159.

Shearer, P. M., Orcutt, J., 1986. Compressional and shear-wave anisotropy in the oceanic lithosphere - the Ngendei seismic refraction experiment. Geophys J Roy Astr S 87 (3), 967–1003.

Silver, P. G., Chan, W. W., 1991. Shear-wave splitting and subcontinental mantle deformation. J Geophys Res-Sol Ea 96 (B10), 16429–16454.

Silver, P. G., Savage, M., 1994. The interpretation of shear-wave splitting parameters in the presence of two anisotropic layers. Geophys J Int 119 (3), 949–963.

Smith, W., Sandwell, D., 1997. Global sea floor topography from satellite altimetry and ship depth soundings. Science 277 (5334), 1956–1962.

Sparks, D., Parmentier, E., Phipps Morgan, J., 1993. Three-dimensional mantle convection beneath a segmented spreading center: implications for along-axis variations in crustal thickness and gravity. J Geophys Res-Sol Ea 98 (B12), 21977–21995.

Teanby, N., Kendall, J. M., der Baan, M. V., 2004. Automation of shear-wave splitting measurements using cluster analysis. B Seismol Soc Am 94 (2), 453–463.

Thomsen, L., 1986. Weak elastic anisotropy. Geophysics 51 (10), 1954–1966.

Tommasi, A., 1998. Forward modeling of the development of seismic anisotropy in the upper mantle. Earth Planet Sci Lett 160 (1-2), 1–13.

Tommasi, A., Tikoff, B., Vauchez, A., 1999. Upper mantle tectonics: three-dimensional deformation, olivine crystallographic fabrics and seismic properties. Earth Planet Sci Lett 168 (1-2), 173–186.

van Wijk, J., Blackman, D., 2005. Deformation of oceanic lithosphere near slow-spreading ridge discontinuities. Tectonophysics 407 (3-4), 211–225.

Weatherley, S. M., Katz, R. F., 2010. Plate-driven mantle dynamics and global patterns of mid-ocean ridge bathymetry. Geochem Geophy Geosy 11, Q10003.

Wessel, P., Smith, W., 1991. Free software helps map and display data. EOS Trans. AGU 101, 8415–8436.

Wolfe, C., Silver, P. G., 1998. Seismic anisotropy of oceanic upper mantle: Shear wave splitting methodologies and observations. J Geophys Res-Sol Ea 103 (B1), 749–771.

Wolfe, C., Solomon, S., 1998. Shear-wave splitting and implications for mantle flow beneath the MELT region of the East Pacific Rise. Science 280 (5367), 1230–1232.

Wookey, J., Kendall, J. M., 2004. Evidence of midmantle anisotropy from shear wave splitting and the influence of shear-coupled p waves. J Geophys Res-Sol Ea 109 (B7), B07309.

Wookey, J., Kendall, J. M., 2008. Constraints on lowermost mantle mineralogy and fabric beneath Siberia from seismic anisotropy. Earth Planet Sci Lett 275 (1-2), 32–42.

Wookey, J., Kendall, J. M., Rümpker, G., 2005. Lowermost mantle anisotropy beneath the north Pacific from differential S–ScS splitting. Geophys J Int 161 (3), 829–838.

Wuestefeld, A., Al-Harrasi, O., Verdon, J. P., Wookey, J., Kendall, J. M., 2010. A strategy for automated analysis of passive microseismic data to image seismic anisotropy and fracture characteristics. Geophysical Prospecting 58 (5), 753–771.

Yuan, H., Romanowicz, B., 2010. Lithospheric layering in the North American craton. Nature 466 (7310), 1063–U68.
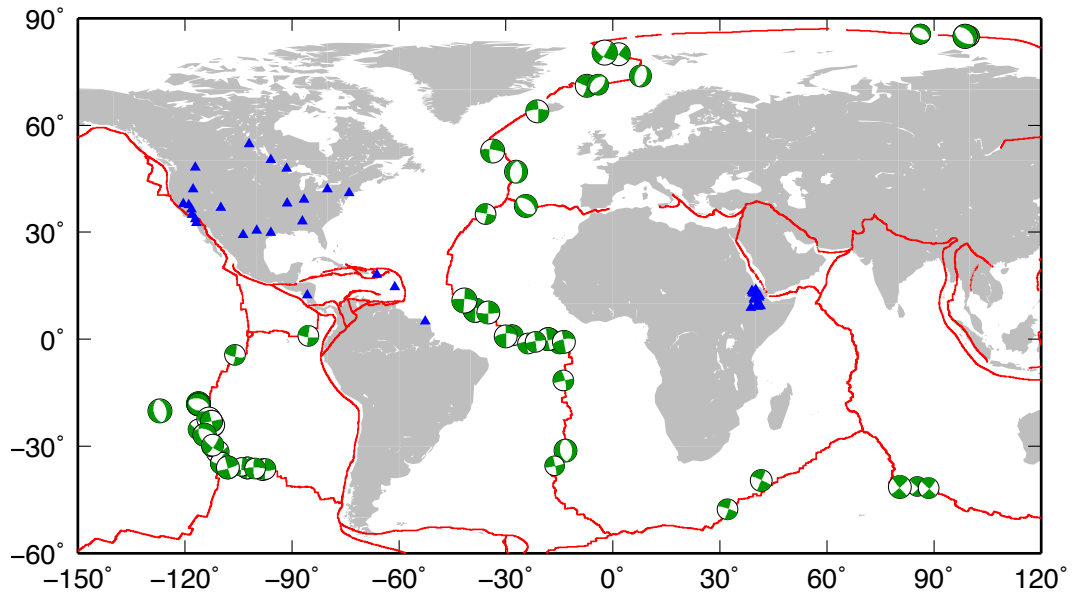
Figure 1: Location of events used in this study with plate boundaries of Bird (2003). Lower-hemisphere focal mechanisms are the best-fitting double-couple solutions as given by the Global CMT project. Blue triangles are seismic stations. Magnitude range ($4.4 \leq M_b \leq 6.7$) shown by size of hemispheres.
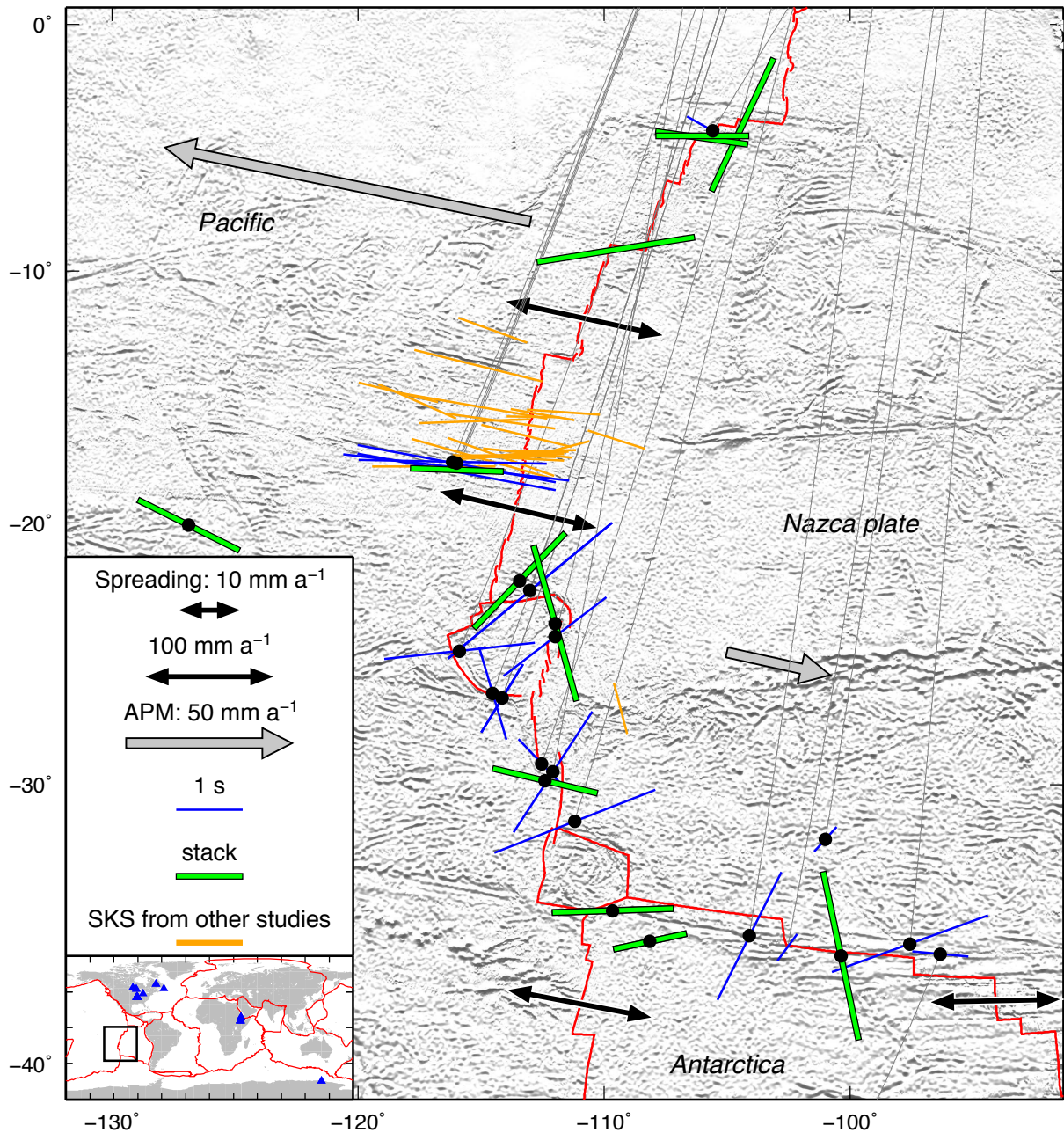
Figure 2: Source-side splitting beneath events on the EPR. Dots show earthquake locations, with bars indicating splitting parameters, where the orientation shows ϕ'' and the length δt, as in the legend. Blue bars are for single measurements; green for stacks. Orange bars show SKS splitting parameters from previous studies (Wolfe and Solomon, 1998; Harmon et al., 2004). Thin grey lines show raypaths to stations (blue triangles, inset map). Shading indicates bathymetry (Smith and Sandwell, 1997), and thin red lines are plate boundaries. Black double-headed arrows show base-10 logarithm of NUVEL-1A full spreading rates at selected locations along the ridge. Grey arrows show the absolute plate motion (APM) in the HS3 reference frame of the NUVEL-1A model (Gripp and Gordon, 2002). The legend indicates spreading and APM rates. Results include stacks from Nowacki et al. (2010).
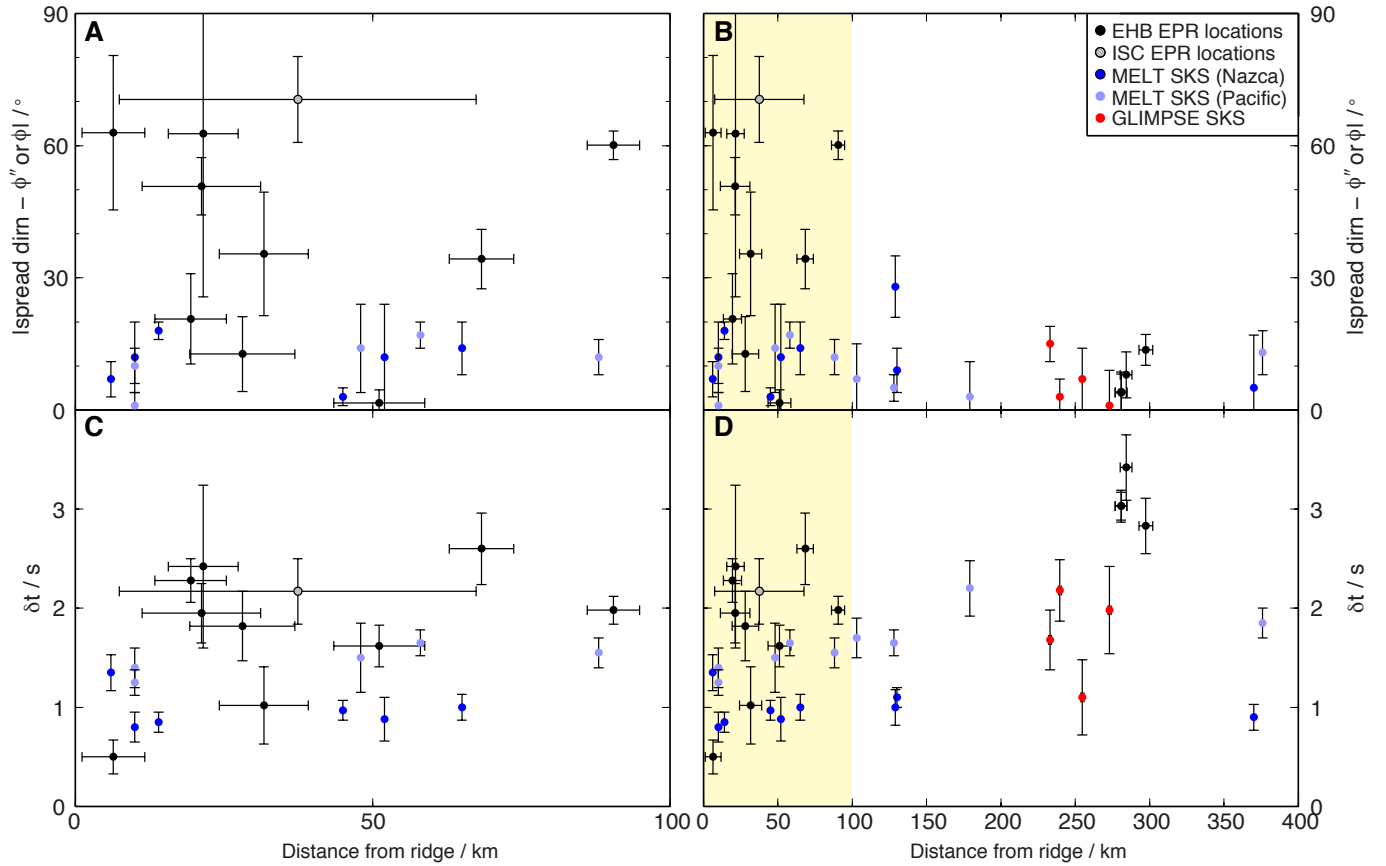
28

Figure 3: Variation of splitting parameters beneath 'ridge' events with distance away from the axial ridge at the EPR. Black and grey circles indicate respectively the EHB and standard ISC locations of the events in this study. Error bars show 95% confidence interval in splitting parameters and stated uncertainty in event locations. Coloured circles indicate MELT (blue) and GLIMPSE (red) SKS splitting parameters as shown in the legend, where MELT stations on the Pacific and Nazca plates are coloured lighter and darker respectively. All GLIMPSE stations are on the Pacific plate. Shaded part of panels on right shows regions shown by panels on left. A) and B) Modulus of difference in angle between ϕ'' or ϕ_{SKS} and the plate spreading direction (DeMets et al., 1994). C) and D) Splitting times for S or SKS.
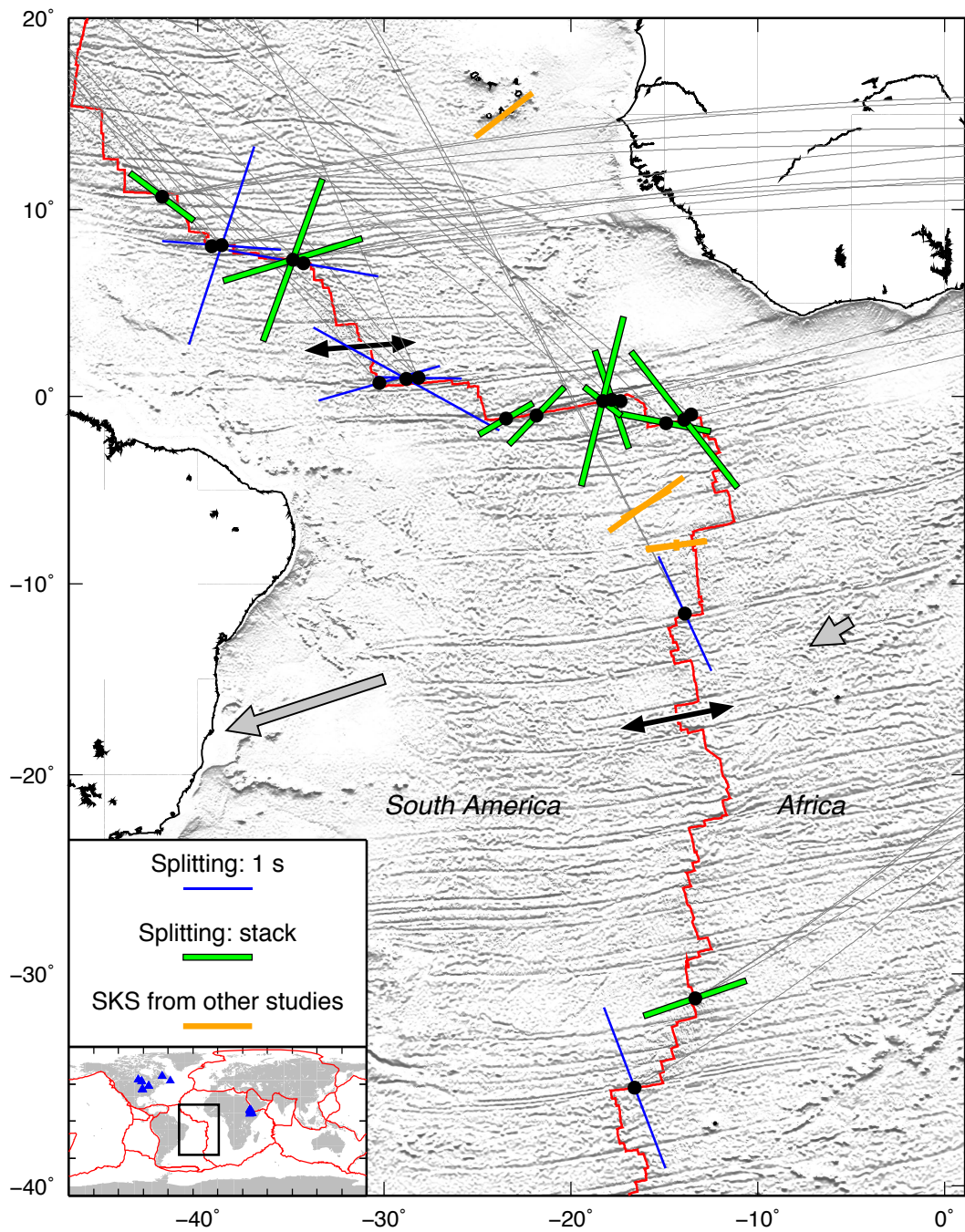
Figure 4: Splitting parameters beneath events on the MAR. Symbols as for Figure 2. Orange bars show SKS results of Wolfe and Silver (1998) and Behn et al. (2004). Note that some events are measured at stations in both North America and Ethiopia, in which case stacks of results for both directions are shown. Spreading rates and APM are of same scale as Figure 2.
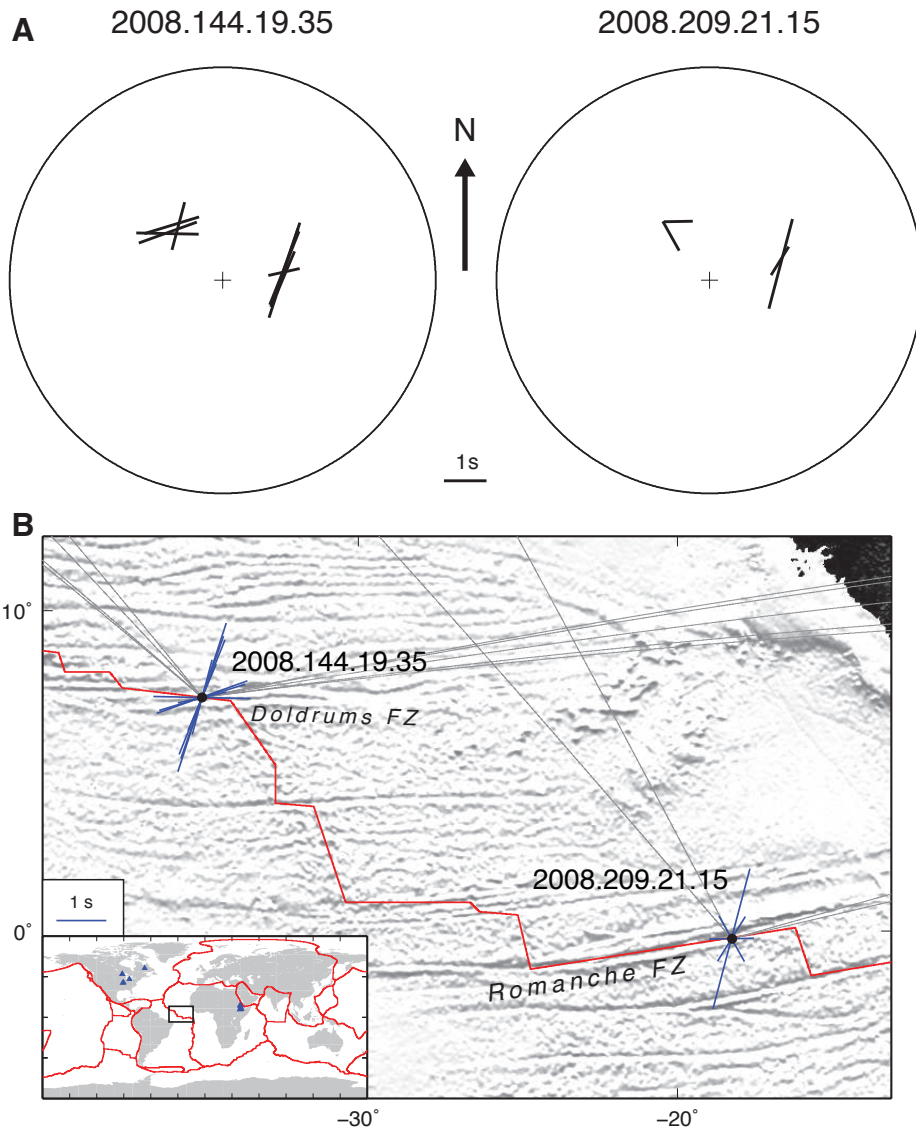
Figure 5: Lower-hemisphere diagrams for splitting parameters measured beneath two events on the MAR. A) Azimuthal and inclination-dependence of splitting parameters shown on equal-area lower-hemisphere projections. Average inclination of downgoing rays in top 150 km of IASP91 (Kennett and Engdahl, 1991) is shown by radial distance (with vertical at the centre). Azimuth corresponds to azimuth at the event. Bar orientation and length corresponds to ϕ'' and δt respectively, as per the scale, centre. The splitting times measured at Ethiopian stations (group on right of hemispheres) are larger for both events, and ϕ'' is also different. B) Location of events and individual splitting measurements shown at earthquake location. Bars correspond to splitting parameters as for previous figures, with delay time indicated by length as per the legend (left). Inset map show location of larger map by thick black box. The raypaths to Ethiopia run along the transform zones, whilst those to North America move away from the transforms.
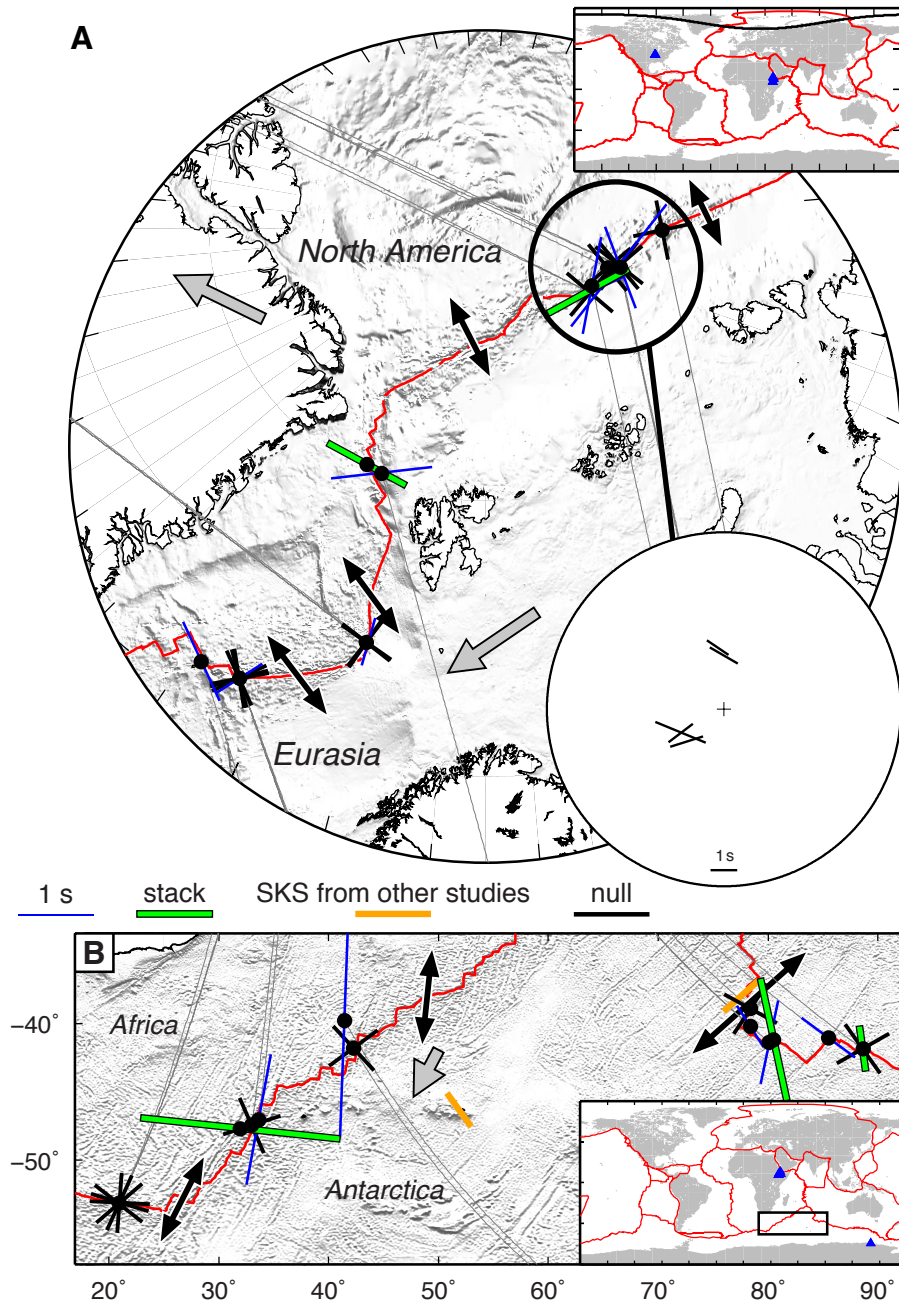
Figure 6: Splitting parameters beneath events on the Gakkel, Southeast and Southwest Indian Ridges. Symbols as for Figure 2, except null results are shown by black crosses with bars parallel to the null directions. A) Results for events on Gakkel Ridge. Thick black circle shows results included in lower hemisphere stereoplot, inset lower right. Bars above the centre show measurements made at North American stations; those to the lower left show measurements at Ethiopian stations. Scale indicated at bottom. B) Results for events on Southwest and Southeast Indian Ridges. SKS splitting at CRZF (Base Alfred Faure, Crozet Islands) and AIS (île Nouvelle-Amsterdam; Behn et al., 2004) is shown by the orange bar. APM is less than 10 mm a^{-1} for African plate, and parallel to spreading direction at ∼65 mm a^{-1} for Australian plate (northeast corner, not labelled).
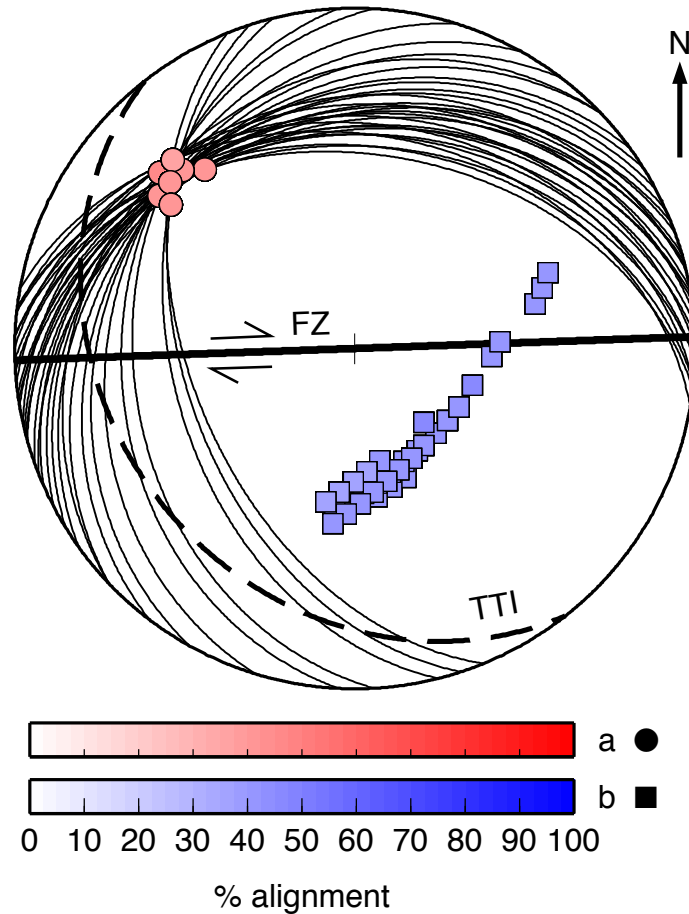
Figure 7: Orientations of olivine a- and b-axes compatible with observations from event 2008.144.19.35 on the Doldrums FZ, MAR. Lower-hemisphere equal area plot shows north upward and the vertical direction out of the page. Red circles (a-axes) and blue squares (b-axes) are shaded per the degree of alignment according to the scale below. Thick black solid line shows approximate strike of FZ and spreading direction, with strike-slip arrows indicating sense of shear. Thick dashed line is best-fitting plane of isotropy from fit of TTI to fast orientations. Thin solid lines are crystallographic slip planes (b-planes) for the case of 'A-type' olivine LPO.
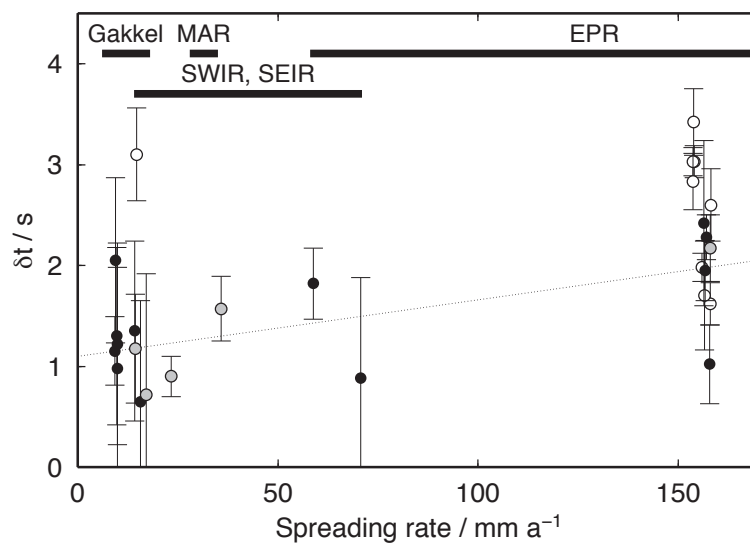
Figure 8: Splitting time versus spreading full-rate beneath all 'ridge' events. Filled circles show results less than 50 km from the ridge axis: black circles shows events with EHB locations; grey circles indicate ISC locations. Open circles indicate events >50 km from the axis (all EHB locations). Thick bars show range of spreading rates represented by events beneath each MOR in this study. Weighted linear fit to near-axis (filled circles) data is shown with thin dotted line.